



ALMA MATER STUDIORUM
UNIVERSITÀ DI BOLOGNA

ARCHIVIO ISTITUZIONALE
DELLA RICERCA

Alma Mater Studiorum Università di Bologna Archivio istituzionale della ricerca

Assessment of high-enthalpy composite eutectic phase change materials efficiency in asphalt binders for cooling pavements

This is the final peer-reviewed author's accepted manuscript (postprint) of the following publication:

Published Version:

Dai, J., Feng, M.a., Sangiorgi, C., Tarsi, G., Zhen, F.u., Tataranni, P., et al. (2024). Assessment of high-enthalpy composite eutectic phase change materials efficiency in asphalt binders for cooling pavements. JOURNAL OF CLEANER PRODUCTION, 442, 1-14 [10.1016/j.jclepro.2024.140999].

Availability:

This version is available at: <https://hdl.handle.net/11585/956413> since: 2024-02-09

Published:

DOI: <http://doi.org/10.1016/j.jclepro.2024.140999>

Terms of use:

Some rights reserved. The terms and conditions for the reuse of this version of the manuscript are specified in the publishing policy. For all terms of use and more information see the publisher's website.

This item was downloaded from IRIS Università di Bologna (<https://cris.unibo.it/>).
When citing, please refer to the published version.

(Article begins on next page)

1 **Assessment of high-enthalpy composite eutectic phase change** 2 **materials efficiency in asphalt binders for cooling pavements**

3 Jiasheng Dai ^{a,b}, Feng Ma ^{a,*}, Cesare Sangiorgi ^b, Giulia Tarsi ^b, Zhen Fu ^c, Piergiorgio Tataranni ^b,
4 Chen Li ^a, Yingjie Hou ^a

5 ^a Key Laboratory for Special Area Highway Engineering of Ministry of Education, Chang'an
6 University, Xi'an, Shaanxi, 710064, China

7 ^b Department of Civil, Chemical, Environmental and Materials Engineering, University of Bologna,
8 Bologna, 40131, Italy

9 ^c School of Material and Science Engineering, Chang'an University, Xi'an, Shaanxi, 710064, China

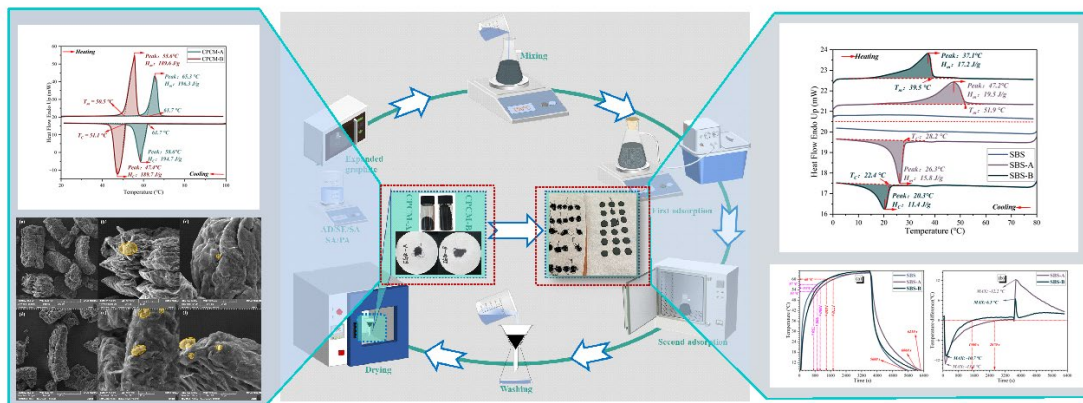
10 *Correspondence: mafeng@chd.edu.cn

11 **Abstract:** Phase change materials (PCMs) as thermal energy storage solutions can mitigate
12 pavement damage and alleviate the urban heat island effect. A stable shape, suitable melting
13 temperature, and high-enthalpy can extend the application potential of PCMs in cooling pavements.
14 The goal behind this study is to investigate the potential use of two high-enthalpy composite phase
15 change materials (CPCMs) in an SBS-modified asphalt binder through thermal and chemo-
16 rheological tests. Herein, using a ternary eutectic mixture with adipic/sebacic/stearic acids (named
17 A) and a binary eutectic mixture consisting of stearic/palmitic acids (named B) as two distinct PCMs
18 and expanded graphite as supporting material, two novel CPCMs were successfully prepared
19 through vacuum impregnation. The findings showed that the encapsulation efficiency of both
20 CPCM-A and CPCM-B exceeded 90%. The melting enthalpy (H_m) and the melting phase-change
21 temperatures (T_m) values were 193.3 J/g and 61.7°C for CPCM-A, 189.6 J/g, and 50.5°C for CPCM-
22 B. The H_m of the two related asphalt binders that incorporate the developed CPCMs (SBS-A and

23 SBS-B) were 19.5 J/g and 17.2 J/g, respectively, indicating high thermal storage and management
 24 capabilities. This allowed SBS-A and SBS-B to exhibit maximum temperature differences of 13.1°C
 25 and 10.7°C, with temperature lags of 1500 s and 2610 s, respectively. Also, the CPCMs and the
 26 related asphalt binders presented outstanding thermal and chemical stability. The CPCMs enhanced
 27 the resistance to deformation and deformation recovery capability of asphalt at high temperatures
 28 and under severe loads. However, SBS-B experienced an earlier phase transition than SBS-A,
 29 ultimately leading to a diminished ability to withstand deformation at the testing temperature. To
 30 sum up, opting for CPCM-A over CPCM-B for asphalt pavement cooling applications is advisable.

31 **Keywords:** Cooling pavements; composite phase change materials; asphalt binders; thermal-
 32 regulating properties; rheological characterization

33 **Graphical Abstract:**



34

35 **1. Introduction**

36 The urbanization process has caused the emergence of the urban heat island (UHI) effect,
 37 whereby urban areas are generally warmer than the surrounding rural environment, especially
 38 during summer (Anupam et al., 2023). This phenomenon is attributed to several factors, including
 39 the use of certain building materials, the complex geometry of urban landscapes, reduced vegetation
 40 cover, and increased anthropogenic heat emissions (Nwakaire et al., 2020). Among all factors, the

41 low reflectivity of black asphalt pavements is one of the leading contributors to the UHI effect, as
42 it absorbs a significant proportion of solar radiation, which turns into high pavement-surface
43 temperatures up to 60°C during summer (Wang, C. et al., 2021). The UHI poses considerable health
44 risks to urban residents, including heat-related illnesses and fatalities (Anderson and Bell, 2011).
45 Additionally, asphalt pavements' viscoelastic and temperature-susceptible properties make them
46 prone to several damages when exposed to prolonged high temperatures (Chen et al., 2020). These
47 damages include rutting and thermo-oxidative aging, which eventually affect the durability and
48 serviceability of road pavements (Yuan et al., 2023a).

49 To ensure that cities are livable with enhanced environmental quality and sustainable energy
50 consumption patterns, it is imperative to adopt UHI mitigation strategies to address these pavement-
51 related adverse consequences, such as installing reflecting and permeable pavements (Gong et al.,
52 2023; Zhang, D.R. et al., 2023). However, such strategies may affect pedestrians' thermal comfort,
53 increasing building energy consumption and carbon emissions (Li et al., 2013). Pavement design
54 that integrates renewable energy technologies, such as latent heat structures and photovoltaic
55 materials, has emerged as a promising approach to mitigate UHI (Guo et al., 2020; Yuan et al.,
56 2023b). These systems achieve surface temperature reduction by converting absorbed radiation into
57 different kinds of energy.

58 A different solution for mitigating the UHI is represented by phase change materials (PCMs).
59 The PCMs are functional materials that have the innate capability to absorb and release thermal
60 energy during their phase transition, offering a potential mechanism for the regulation of
61 temperature variances within pavement structures (Ye et al., 2014). Such thermoregulatory attributes
62 can extend the longevity of road pavements by mitigating the frequency of thermally induced

63 mechanical stresses (Zhang, J. et al., 2023). Concurrently, when integrated into pavement systems,
64 the PCMs can incorporate superfluous thermal energy at maximal temperatures achieved during the
65 daytime, resulting in a marked reduction of the pavement's surface temperature (Wu et al., 2022).
66 Subsequently, as temperatures decrease, particularly during cooler periods like nighttime, phase
67 change materials (PCMs) progressively discharge the accumulated thermal energy. Although this
68 released heat energy leads to an elevation in pavement temperature, the gradual discharge of heat
69 aids in regulating ambient temperatures, leading to a more consistent thermal environment in
70 comparison to the rapid heat release from conventional surfaces (Roman et al., 2016; Salem and
71 Bichara, 2023). Their application in urban structures also helps mitigate the UHI by moderating
72 surface temperatures and minimizing temperature fluctuations within urban environments.,
73 presenting a viable strategy to counteract the UHI (Kakar et al., 2019b; Tyagi et al., 2021).

74 Therefore, it may be feasible to depend on the phase-change thermal characteristics of PCMs
75 to endow the pavement with latent heat ability, thereby alleviating the temperature stress and UHI.
76 Zhang et al. (Zhang, J. et al., 2023) incorporated 4% paraffin/expanded graphite/high-density
77 polyethylene composites into asphalt binder, showing a temperature difference of 4°C and a delay
78 time of 456 s. Polyurethane solid-solid PCMs were synthesized by Jia et al. (Jia et al., 2023), Liu et
79 al. (Liu et al., 2023), and Jiao et al. (Jiao et al., 2023) to equip asphalt binder with thermal regulation
80 properties and decrease the temperature of road pavements. According to previous researches, the
81 integration of expanded graphite (EG)/polyethylene glycol (PEG) as composite phase change
82 materials (CPCMs) into asphalt binders resulted in enhanced resistance to rutting and noticeable
83 cooling effect (Zhang, D. et al., 2018; Zhang et al., 2019). Meanwhile, Jin et al. (Jin et al., 2021; Jin
84 et al., 2018) utilized diatomite and stearic acid (SA) to develop excellent chemical and thermal

85 stability CPCMs. This innovative approach decreased the temperature of the upper and lower
86 surfaces of asphalt pavement by 10.90°C and 5.03°C, respectively. Farnam et al. (Farnam et al.,
87 2016) integrated lightweight aggregates with PCM into the pavement, resulting in a significant
88 maximum heat release potential of 12.11 kJ/m³. Furthermore, Dai et al. (Dai et al., 2021; Dai et al.,
89 2022), Jia et al. (Jia et al., 2021), Du et al. (Du et al., 2019), and Kakar et al. (Kakar et al., 2019a)
90 reported that the direct introduction of PCM would soften the asphalt binder due to the liquefaction
91 after the phase transition of PCM, resulting in a significant decrease in both its viscosity and
92 elasticity. Obviously, the previous research presented a viable approach for utilizing PCM for
93 pavement cooling. Nevertheless, some obstacles might significantly constrain its widespread
94 implementation, such as unreasonable encapsulation strategies, mismatched melting temperature,
95 low-enthalpy, etc. Further studies on the utilization of PCMs in cooling pavements mainly revolve
96 around two subjects: the selection of PCM and the encapsulation technology. Table 1 compiles the
97 findings of investigations on using CPCMs in cooling pavements. It can be concluded that the
98 methods of CPCMs preparation primarily include chemical synthesis, microencapsulation, and
99 vacuum adsorption, with an enthalpy of below 100 J/g. Moreover, the selection of PCM mainly
100 focuses on PEG, SA, and paraffin. However, phase change temperature and enthalpy are two
101 inherent features of PCM (Hasanabadi et al., 2021). It is challenging to find naturally occurring
102 solid-liquid PCMs that meet both a reasonable phase change temperature and a high enthalpy (Bai
103 et al., 2018). Therefore, developing an ideal CPCM with the maximum possible enthalpy,
104 appropriate phase change temperature, and stable packaging technology is imperative.

105 Table 1 Summary of preliminary research on the application of CPCMs in cooling pavements

PCMs	Supporting materials	Encapsulation Technology	Phase change temperature (°C)	Phase change enthalpy (J/g)	Ref.
PEG-800	Polyacrylamide	Graft copolymerization	17.10	72.2	(Cheng et al., 2021)
PEG-1000	Diatomite	Vacuum adsorption	40.12	67.48	(Wang, H. et al., 2021)
PEG-2000	Lightweight aggregate	Vacuum adsorption	53.00	7.96-17.69	(Yinfei et al., 2020)
PEG-2000	Cement	Polymeric hydration	53.59	37.47	(Du, Y. et al., 2021)
PEG-2000	Hydrophobic fumed silica	Sol-gel	50.00	173.60	(Hu et al., 2021)
PEG-2000	Expanded graphite	Vacuum adsorption	45.33-50.07	120.45-137.94	(Zhang, D. et al., 2018)
PEG-4000	Silica	Sol-gel	62.80	48.50	(Chen et al., 2019)
PEG-4000	-	Chemical bonding	25.60-45.70	58.60-128.40	(Liu et al., 2023)
PEG-8000	-	Chemical bonding	50.20	115.20	(Jia et al., 2023)
Paraffin	Expanded perlite	Vacuum adsorption	62.30	76	(Hasanabadi et al., 2021)
Paraffin	high-density polyethylene	--	11.00-37.00	186.00	(Zhang, J. et al., 2023)
Paraffin	Polyurethane/epoxy resin	One-step	-0.33	14.40	(Bai et al., 2018)
SA	Montmorillonite	-	40.00-85.00	221.60	(Liu et al., 2022)
SA	Mineral-supported	Vacuum adsorption	66.77-67.13	105.50-143.7	(Jin et al., 2021)
Pentadecane	Nano-silica and ethyl cellulose	Microencapsulation	15.30	117.40	(Ma et al., 2019)

106 On top of that, the use of eutectic technique for PCMs is a compelling advancement in the
107 ongoing researches, as it enables customization of the melting point to meet specific requirements
108 (Du, W. et al., 2021). The eutectic technique involves blending two or more fatty acids in a particular
109 mass proportion to achieve the least possible melting point, which considerably simplifies the task
110 of matching PCMs while expanding their higher latent heat (Yang et al., 2019). A set of multiple
111 eutectic mixes based on fatty acids with 10-18 carbons was described by Ke et al. (Ke, 2017) and
112 Nazir et al. (Nazir et al., 2018), with phase change temperatures between 15°C and 50°C.
113 Furthermore, some naturally dicarboxylic acids (DA), such as adipic acid (AD) and sebacic acid
114 (SE), possess the advantages of being cost-effective, abundantly available, and having a high
115 enthalpy. However, their usage is limited due to their high melting point (AD-152.1°C, SE-134.5°C)
116 (Haillet et al., 2011; Kolyado et al., 2016). Eutectic technology can incorporate these DA into

117 asphalt pavements. Ma et al. (Ma et al., 2018) reported the thermal properties and stability of three
118 binary eutectic mixtures of AD/SA, SE/SA, and suberic acid/SA binary eutectic PCMs, with the
119 following melting temperatures: 67.45°C, 66.37°C, and 67.08°C. Seki et al. (Seki et al., 2015)
120 employed graphite nanosheets to load an AD/SE eutectic mixture, achieving a melting temperature
121 of 116°C. Nevertheless, literature is lacking concerning using DA in cooling pavements. Moreover,
122 EG is a novel carbon-based material with impressive attributes such as exceptional thermal
123 conductivity, absorption capacity, thermal stability, and compatibility (Zhang, D. et al., 2018). The
124 EG can serve as a PCM-supporting material to mitigate the leakage of PCM itself and enhance heat
125 transfer efficacy. Hence, exploiting the positive experience of eutectic PCM in thermal energy
126 storage is a forward-thinking approach to developing an asphalt pavement with temperature-
127 regulating capability.

128 In the present study, two high-enthalpy CPCMs were developed employing vacuum
129 impregnation, using AD/SE/SA and SA/PA eutectic mixtures as phase change units and EG as
130 supporting material. Notably, AD and SE were first introduced into asphalt pavements as energy
131 storage materials. Initially, the phase change behavior, and thermal and chemical stability of the two
132 CPCMs were assessed. Then, the CPCMs were integrated into the SBS-modified asphalt binder,
133 and the resulting binders underwent thermal and chemo-rheological characterizations.

134 **2. Materials and test methods**

135 **2.1 Raw Materials**

136 2.1.1 Asphalt binder

137 Styrene-butadiene-styrene (SBS) polymer-modified asphalt, graded as 40/100-55, produced
138 by an Italian company, was used as a base and control binder in this research. The conventional

139 physical properties of the soft modified asphalt binder provided by the supplier are listed in Table
 140 2.

141 Table 2 Physical properties of SBS-modified bitumen 40/100-55 (from the technical data sheet)

Characteristics	Property	Method	Unit	Performance	
				min	max
Consistency at intermediate service temperatures	Penetration at 25°C	EN 1426	dmm	45	70
Consistency at high service temperatures	Softening Point P.A.	EN 1427	°C	55	
Cohesion	Force Ductility Test at 5°C	EN 13589 EN 13703	J/cm ²	3.0	
Durability Resistance to RTFOT aging	Mass variation	-	%		0.8
	Residual penetration at 25°C	EN 1426	%	50	
	Δ Softening point	EN 1427	°C		10
Flammability	Flash point	EN ISO 2592	°C	250	
Dynamic viscosity	Viscosity at 160°C	EN 13302	Pa.s	0.30	
Deformation recovery	Elastic Return at 25°C	EN 13398	%	60	
Storage stability/EN13399	Δ Softening point	EN 1427	°C		5
	Δ Penetration at 25°C	EN 1426	dmm		9

142 2.1.2 Fatty acids

143 Four fatty acids were selected as PCMs provided by Shanghai Macklin Biochemical
 144 Technology Co., Ltd, including palmitic acid (PA), stearic acid (SA), sebacic acid (SE), and adipic
 145 acid (Ad). Some of their information is listed in Table 3. The supplier furnished the essential data,
 146 while a differential scanning calorimeter (DSC) determined the phase change temperature and
 147 enthalpy.

148 The abovementioned materials were combined to produce two high-enthalpy PCMs. One
 149 ternary and one binary eutectic mixture were developed as phase change units: AD/SE/SA and
 150 SA/PA. The two PCMs are coded as A and B, respectively.

151 Table 3 Information on fatty acids

Item	CAS No	Linear Formula	Molecular Weight	Purity (%)	Phase-change temperature (melting, °C)	Phase-change enthalpy (melting, °C)
PA	57-10-3	CH ₃ (CH ₂) ₁₄ COOH	256.42	99	61.10	213.29
SA	57-11-4	CH ₃ (CH ₂) ₁₆ COOH	284.48	98	67.70	223.75
SE	124-04-9	HOOC(CH ₂) ₄ COOH	146.14	≥98	151 - 154	267.55
AD	111-20-6	HOOC(CH ₂) ₈ COOH	202.25	99	133 - 137	247.83

152

153 2.1.3 Expanded graphite

154 Expanded graphite (EG) was used as a supporting material for the two PCMs. The used
 155 expanded graphite has a particle size of 80 mesh, an expansion rate of 200 to 350 times, and a purity
 156 level of 99%.

157 2.2 Determination of the mass proportion of binary/ternary eutectic phase change 158 materials (PCMs)

159 The theoretical molar ratio of a mixture was determined using the Schrader Equations (1 and
 160 2), derived from the second law of thermodynamics and phase equilibrium theory (Kolyado et al.,
 161 2016). Then, the theoretical molar ratios of the SA/PA binary eutectic mixture and AD/SE/SA
 162 ternary mixture were translated to theoretical mass ratios (Ke, 2017; Nazir et al., 2018). When
 163 calculating the eutectic point for a ternary mixture, the AD/SE binary mixture was treated as a new
 164 single pure component, and a third phase (SA) was introduced to form AD/SE/SA ternary eutectic
 165 mixture.

$$166 \ln X_i = \frac{\Delta H_i}{R} \left(\frac{1}{T_i} - \frac{1}{T} \right) \quad (i = A, B) \quad (1)$$

$$167 X_A + X_B = 1 \quad (2)$$

168 Where, X_i is the mole percentage of component i , T_i is the melting temperature of
169 component i (K), R is the gas constant (8.314 J/(mol·K), and ΔH_i is the molar heat of fusion
170 of component i (J/mol).

171 Based on this, the mass ratios of the AD/SE/SA ternary mixture and SA/PA binary eutectic
172 mixture were 0.0305:0.0658:0.9037 and 0.398:0.602, respectively.

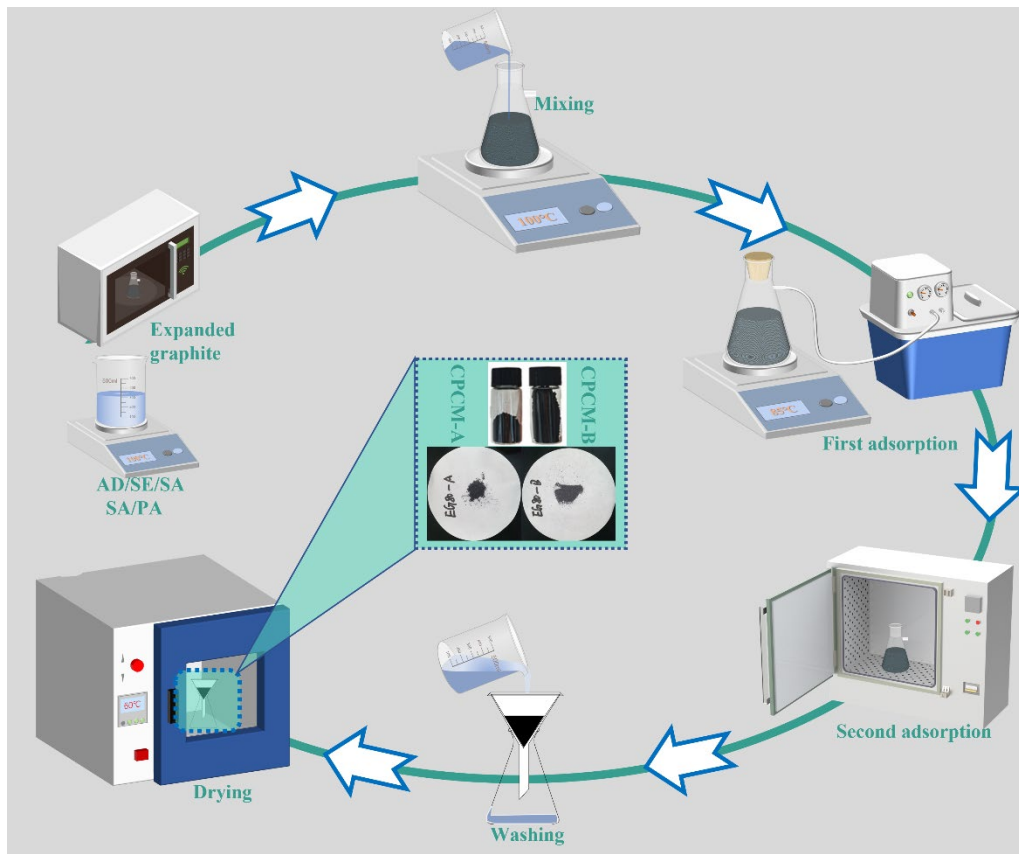
173 **2.3 Preparation of samples**

174 2.3.1 Preparation of composite phase change materials (CPCMs)

175 The melt blending method was used to prepare eutectic mixtures of the two PCMs. The
176 appropriate mass of all fatty acids was placed on an analytical scale with an accuracy of 0.001g, and
177 then, the composite materials were put into a preheated oven at 150°C. When the samples were
178 melted, they were put in a magnetic stirrer and mixed at 300 rpm for 2 h at 100°C to obtain the
179 corresponding binary/ternary eutectic mixture.

180 The CPCMs were synthesized using a vacuum impregnation technique, with the eutectic
181 mixture as the core material and the EG as the supporting one. This involved drying a certain
182 quantity of EG in an oven at 100°C for 24 h to eliminate moisture and rotating it in a microwave
183 oven for two minutes to obtain fully EG. Once ready, the EG was mixed with one of the melted
184 eutectic mixtures in a suction flask, considering a mass ratio of 1:15 (PCM:EG). Then, the suction
185 filter flask was placed on a magnetic stirrer at a temperature of 85°C at 100 rpm and evacuated with
186 a vacuum pump at 0.12 MPa for 4 h to facilitate the impregnation of the eutectic mixture into the
187 pore structure of EG. After this mixing phase, the suction flask was placed in a vacuum oven at
188 85°C for 48 h to ensure the full impregnation of EG with the eutectic mixture. The obtained black
189 mixture was subsequently washed four times with absolute ethanol. Finally, the rinsed sample was

190 placed in an oven at 60°C for 4 h to evaporate absolute ethanol completely. The final dry product
191 obtained is the CPCM, and the detailed synthesis process of CPCM is presented in Figure 1. The
192 same procedure was replicated to produce both CPCM. The two CPCM produced with the ternary
193 and binary eutectic mixtures are indicated as CPCM-A and CPCM-B, respectively.



194
195

Figure 1 The detailed synthesis process of CPCMs

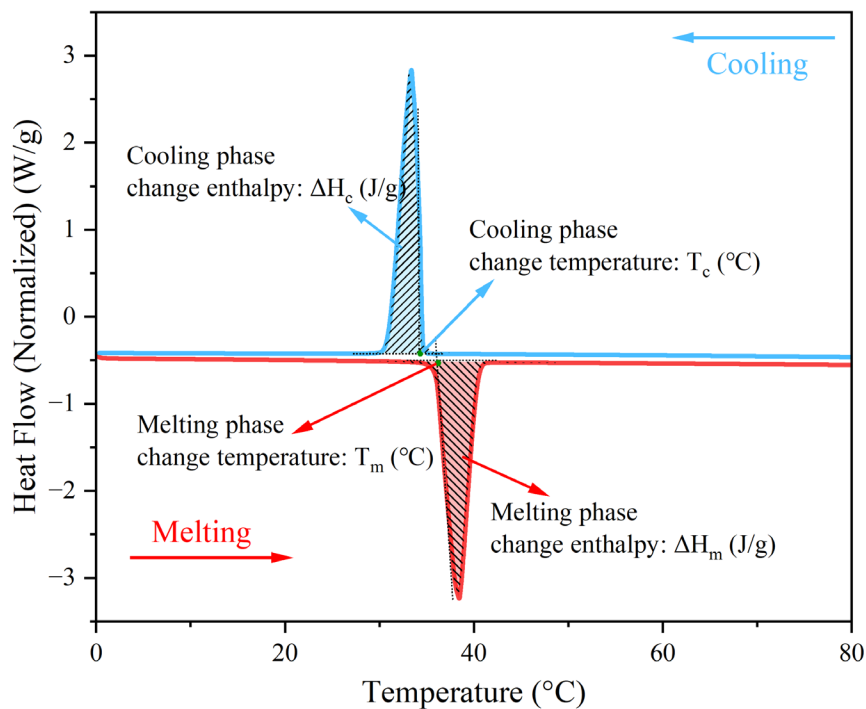
196 2.3.2 Preparation of composite phase change asphalt binders

197 A propeller mixer was used to manufacture the SBS-modified asphalt binders incorporating
198 the two CPCMs. Since 15% SA/PA content had been shown to have little effect on the asphalt
199 binder while exhibiting outstanding temperature regulation performance in our earlier research (Dai
200 et al., 2021; Dai et al., 2022; Dai et al., 2023), both samples were added at that concentration (by
201 mass of original SBS-modified asphalt binder). Following, the CPCMs and the preliminary heated
202 asphalt binder were mixed at 140°C at a mixing rate of 1000 rpm for 30 minutes.

203 2.4 Thermal, chemical, and rheological characterizations

204 2.4.1 Differential scanning calorimeter tests

205 The heat storage and release capabilities of two CPCMs and three asphalt binders (i.e., SBS,
206 SBS-A, and SBS-B) were assessed using a differential scanning calorimeter (DSC, DSC 4000,
207 PerkinElmer). The DSC tests were operated at a heating/cooling rate of 5°C/min in a nitrogen
208 atmosphere while each sample underwent two heating-cooling cycles within the temperature range
209 between 0°C and 100°C. A five-minute equilibration period was implemented after each
210 heating/cooling cycle to eliminate any thermal history and reduce measurement errors. Four key
211 thermal parameters, including the variation of melting enthalpy (ΔH_m), melting phase transition
212 temperature (T_m), the variation of cooling enthalpy (ΔH_c), and cooling phase transition temperature
213 (T_c), were defined to provide a clearer description of the sample's phase transition process. For
214 further details, please refer to Figure 2.



215

216

Figure 2 Determination of the phase-change parameters

217 2.4.2 Attenuated Total Reflection Fourier Transform Infrared tests

218 The chemical structure of the two CPCMs and the three asphalt binders was analyzed using
219 the Fourier Transform Infrared Spectrometer (FTIR, Spectrum 3, PerkinElmer) in the attenuated
220 total reflectance (ATR) mode. Measurements were taken in wavelengths from 500 to 4000 cm^{-1} to
221 capture the spectra, performing 32 scans at 4 cm^{-1} for each sample. Two replicates of each sample
222 were carried out.

223 2.4.3 Thermogravimetric tests

224 To ensure the temperature regulation ability of CPCMs in cooling asphalt pavement, they must
225 be endowed with superior thermal stability, which turns into thermal durability in the corresponding
226 working setting. The thermogravimetric analysis instrument (TGA, TGA 4000, PerkinElmer) was
227 used to characterize the thermal stability of the three asphalt binders and the two CPCMs. The
228 experiment was conducted under a nitrogen atmosphere, whereby approximately 20 mg of the
229 sample was heated at a rate of 10°C/min from 30°C to 600°C. The test was replicated two times per
230 specimen.

231 2.4.4 Microstructure analysis

232 Scanning electron microscopy (SEM, MIRA3 TESCAN, Czech Republic) was employed to
233 obtain CPCM-A and CPCM-B microstructure images. To prevent the occurrence of blurry images
234 caused by the low electronic conductivity of the specimens, the CPCMs that were uniformly
235 distributed on the supporting tools underwent metallization treatment using gold (Lecia EM
236 ACE600). The images were captured at an accelerating voltage of 15 kV.

237 2.4.5 Rheological tests

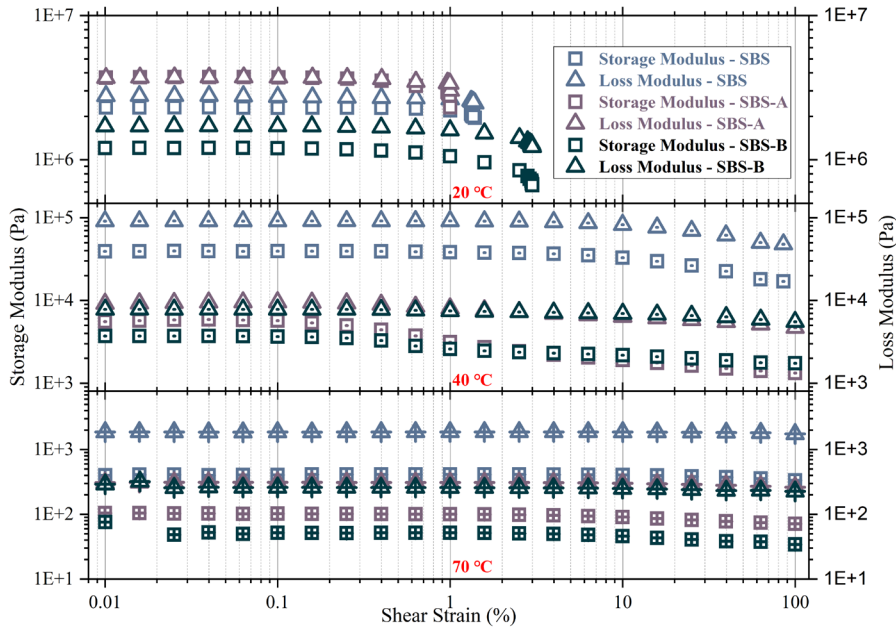
238 The dynamic shear rheometer (DSR, MCR 302, Anton Paar, Austria) was utilized to measure
239 the rheological properties of the asphalt binders. It is common practice to use the DSR to

240 characterize asphalt's viscoelastic properties by measuring several rheological parameters, including
241 complex shear modulus (G^*) and phase angle (δ), of tests run under controlled temperature, loading
242 frequency, and strain magnitude conditions. Samples' preparation and testing apparatus followed
243 the EN 14770 standard using the 25-mm parallel plate geometry with a 1-mm gap setting (ASTM,
244 2015).

245 Preliminarily, the amplitude sweep tests were carried out to define the linear viscoelastic (LVE)
246 range of the asphalt binders at three test temperatures, 20°C, 40°C, and 70°C, and the results are
247 shown in Figure 3. The test temperatures were selected to cover the temperature range between
248 20°C and 70°C at which the temperature sweep tests were performed. The corresponding strain at
249 95% of the initial storage modulus (the elastic component of G^*) has been selected to mark the
250 threshold of non-destructive deformation, i.e., the LVE range. Therefore, to guarantee that the three
251 asphalt binders remained within the LVE range during the temperature sweep tests, a strain of 0.1%
252 was selected. As anticipated, during the temperature sweep tests, the temperature varied between
253 20°C to 70°C at a rate of 2°C/min, while the frequency was maintained at a constant value of 10
254 rad/s.

255 The Multiple Stress Creep and Recovery (MSCR) test followed the ASTM D7405-15 standard.
256 The sample was loaded at a constant stress for 1 s and then allowed to recover for 9 s. Twenty creep
257 and recovery cycles were run at 0.1 kPa, followed by ten creep and recovery cycles at 3.2 kPa. The
258 MSCR tests were conducted at four distinct temperatures (precisely 30°C, 40°C, 50°C, and 60°C)
259 to investigate the phase-change behavior of CPCMs comprehensively. Finally, the data were
260 extracted to calculate the creep parameters: average percent recovery at 0.1 kPa ($R_{0.1}$) and 3.2 kPa
261 ($R_{3.2}$) and the average non-recoverable creep compliance at 0.1 kPa ($J_{nr0.1}$) and 3.2 kPa ($J_{nr3.2}$),

262 according to ASTM D7405-2015. The two parameters at the lowest creep load only considered the
 263 latest 10 cycles. Two replicates were performed in the temperature sweeps and MSCR tests. The
 264 rheological tests were replicated two times per specimen.



265

Figure 3 The linear amplitude sweeps of asphalt binders

266

267 2.4.6 Temperature-time curve tests

268 To assess the thermal regulation capabilities of the three types of asphalt binders, temperature-
 269 time curves were continuously monitored while subjecting the samples to a consistent temperature
 270 of 65°C. Initially, 50 g of the sample was weighed and transferred to a beaker, which was then stored
 271 in a refrigerator at 4°C for 2 h to ensure that all samples were conditioned at the same initial test
 272 temperature. The samples were subsequently placed in an oven and heated until the temperature
 273 stabilized at 65°C. At that point, they were removed and returned to the refrigerator to monitor the
 274 cooling process. The asphalt binders setting and the temperature acquisition instrument are
 275 presented in Figure 4. Two replicates were taken.



276

277

Figure 4 Schematic diagram of temperature acquisition

278 3. Results and discussion

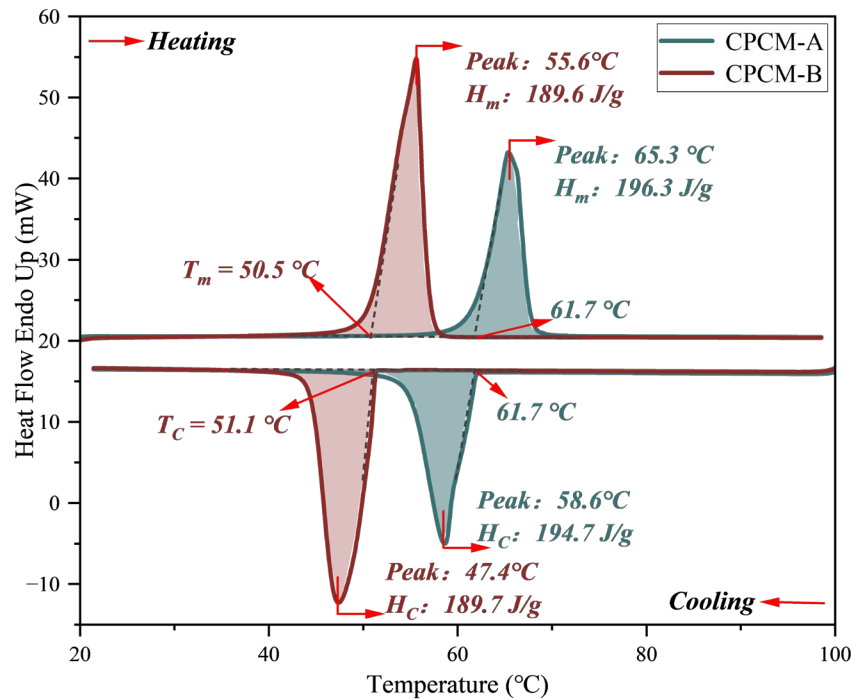
279 3.1 Thermal properties of CPCMs

280 3.1.1 Phase change behaviors of CPCMs

281 The phase-change enthalpy represents a significant parameter when assessing the thermal
282 energy storage potential of a PCM, while the phase-change temperature determines its suitable
283 operational environment (Dai et al., 2023; Hou et al., 2023; Jia et al., 2022). As shown in Figure 5,
284 the heat flow curves of both CPCMs exhibited apparent endothermic and exothermic peaks during
285 the melting and cooling processes, suggesting that the PCMs were effectively encapsulated in EG.
286 The thermal regulation properties of a material are generally enhanced with higher enthalpy values
287 (Wei et al., 2022). The CPCM-A and CPCM-B showcased significant melting enthalpies of 193.3
288 J/g and 189.6 J/g, respectively. Given that the support material, EG, lacks latent heat properties, it
289 was evident that these enthalpies originated from AD/SE/SA and SA/PA. Therefore, the
290 encapsulation efficiency (η), calculated by dividing the melting enthalpy of CPCMs by the melting
291 enthalpy of eutectic PCMs, was derived inversely. With the original melting enthalpies for these
292 eutectic PCMs approximated at 211 J/g, encapsulation efficiencies exceeded 90%. Notably, the

293 phase-change temperatures (T_m) of CPCM-A and CPCM-B were recorded at 61.7°C and 50.5°C,
 294 respectively. Minor reductions in T_m , 2.14°C for CPCM-A and 2.32°C for CPCM-B, may be
 295 attributed to the EG's porous cross-linked network impeding eutectic PCM molecular movements
 296 (Ma et al., 2023). Meanwhile, the melting and cooling stages of the two kinds of CPCMs exhibited
 297 symmetric melting and cooling peaks with no discernible supercooling effect. The supercooling
 298 degrees of CPCM-A and CPCM-B were determined to be 0°C and 0.6°C, respectively, indicating
 299 outstanding crystallization properties. The CPCMs had appropriate crystallization temperatures of
 300 61.7°C and 51.1°C, ensuring their resilience to thermal cycling in asphalt pavement environments.

301 Compared with Table 1, the enthalpy of CPCMs in this work is around 2÷3 times greater
 302 than most of previous studies on this topic (Chen et al., 2019; Liu et al., 2023; Ma et al., 2019; Wang,
 303 H. et al., 2021). These findings highlighted the CPCMs' superior temperature regulation capabilities,
 304 making them prime candidates for enhancing asphalt pavement performances.



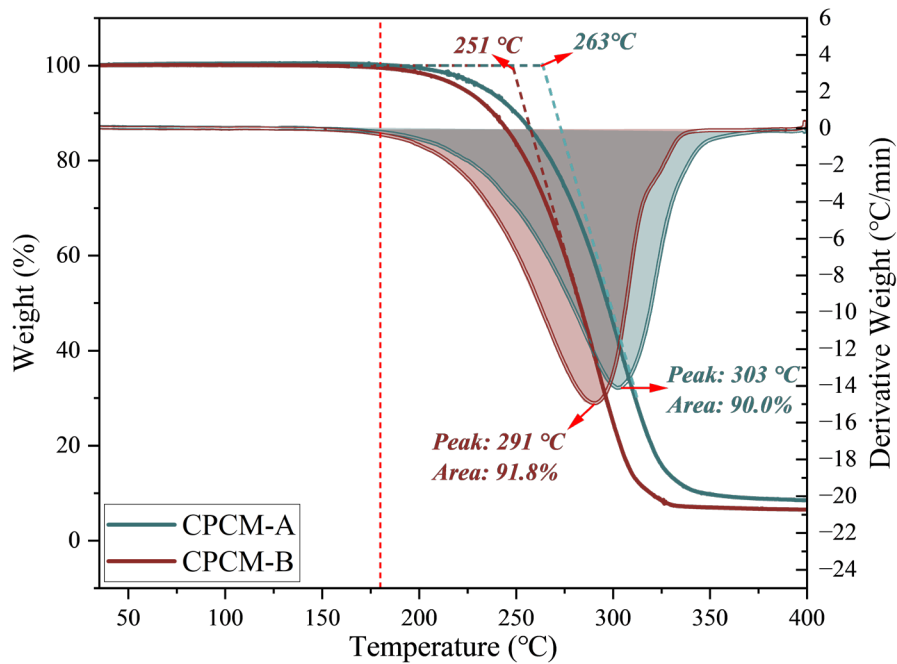
305

306

Figure 5 The heat flow curves of CPCMs obtained from DSC tests

307 3.1.2 Thermal stability of CPCMs

308 The thermal decomposition curves of CPCMs with increasing temperature and their
309 corresponding derivative weight curves are shown in Figure 6. Given that standard operational
310 conditions of asphalt pavements do not exceed 70°C, the crucial threshold temperature of a hot mix
311 asphalt mixtures lies at 180°C (marked by the red line in Figure 6) (Dai et al., 2021). Both CPCM-
312 A and CPCM-B exhibited remarkable thermal stability within the working temperature. Specifically,
313 these CPCMs displayed a mass retention of 100% at 180°C. This indicates their resistance to thermal
314 decomposition at typical mixing temperatures of hot asphalt mixes. Moreover, the onset and
315 completion temperatures for thermal decomposition of the CPCMs were observed at 190°C and
316 350°C, respectively, with the highest decomposition rates detected at 291°C for CPCM-A and 303°C
317 for CPCM-B. Based on these results, it is reasonable to conclude that CPCM-A and CPCM-B have
318 the required thermal stability to meet the demands of the asphalt pavement industry throughout the
319 construction and service stage (Zhang, J. et al., 2023). It is noteworthy that EG exhibited great
320 stability up to 400°C without undergoing any thermal reactions, ensuring a constant quality of the
321 material (Zhang et al., 2021; Zhang, D. et al., 2018). As a result, the weight loss during the thermal
322 decomposition reaction is solely attributed to the eutectic PCMs. This phenomenon is reflected by
323 the peak areas in the derivative weight curve, revealing that CPCM-A and CPCM-B exhibited peak
324 areas of 90.0% and 91.8%, respectively. This reinforces that EG's encapsulation efficiency of
325 eutectic PCMs exceeded 90%.



326

327

Figure 6 The TG and DTG curves of CPCM

328 3.2 Microstructure analysis of CPCM

329 Figure 7 displays the SEM images of CPCM at different magnifications. According to the

330 previous findings (Li et al., 2019; Liu et al., 2014; Zhang, D. et al., 2018), EG with a highly porous

331 structure enhances its ability to adsorb liquefied PCMs. This porous quality is pivotal in applications

332 where high adsorption is desired. From the images, specifically Figures 7 (a) and (d), the worm-like

333 or layered configuration without discernible pore structures of CPCM powder was visible. This

334 specific structural configuration suggested a heightened capability of eutectic PCMs to permeate

335 these structures under a vacuum, hence filling the available voids. This results in a remarkable

336 adsorption capacity, reaching up to 90% for eutectic PCMs. Additionally, the dissolution and

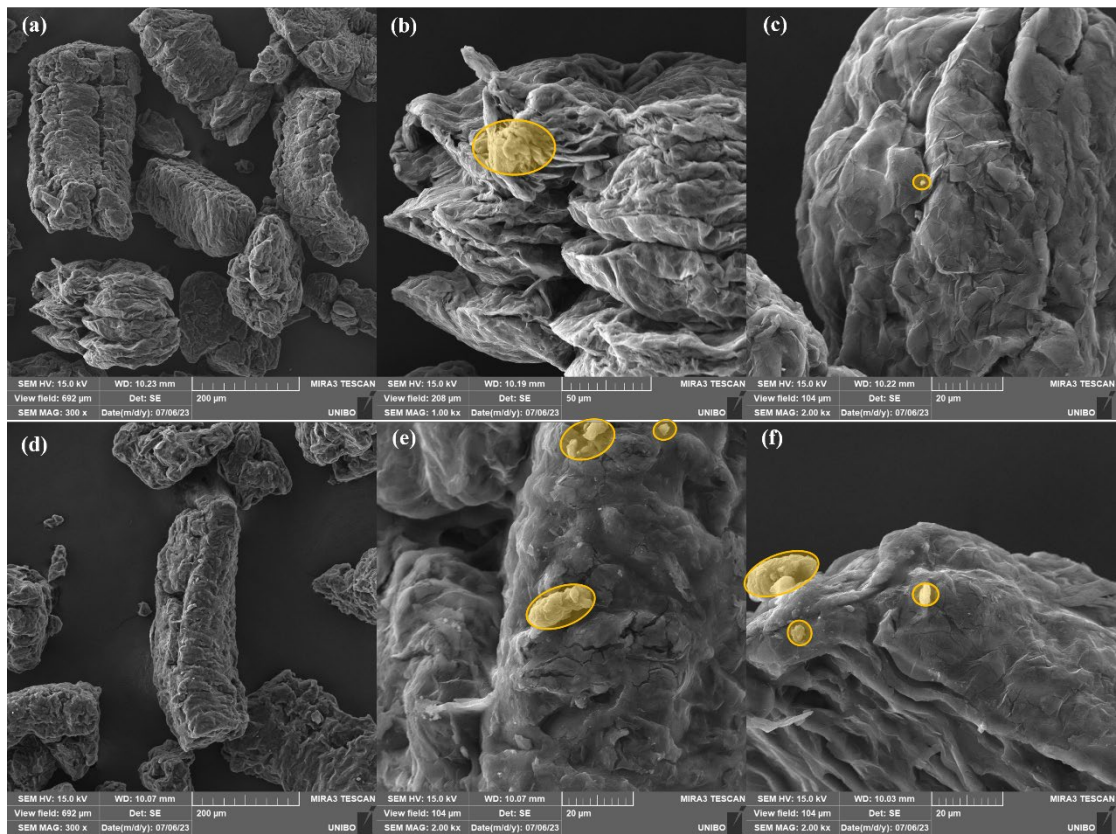
337 washing process using absolute ethanol effectively removed many eutectic PCMs remaining on the

338 external surface of EG particles. This prevents the leakage of eutectic PCMs when EG is subjected

339 to capillary force and surface tension after melting, thereby behaving as solid-solid PCMs on a

340 macroscopic scale. However, as marked by yellow areas in Figures 7 (b), (c), (e), and (f), there were

341 small proportions of unencapsulated or free-eutectic PCMs on EG surfaces. While this fraction is
342 minor, its melting can cause infiltration into the asphalt binder. Even though the impact of this
343 infiltration might be perceived as marginal in the context of asphalt pavement performance,
344 especially in severe environmental conditions, even slight alterations in binder properties may have
345 adverse and cumulative effects over time. This observation might pave the way for future research
346 to optimize the encapsulation process, thus enhancing the long-term performance and durability of
347 the asphalt pavements integrated with these PCMs.



348

349 Figure 7 SEM images of CPCMs: (a), (b), and (c) CPCM-A; (d), (e), and (f) CPCM-B

350 3.3 Chemical stability of CPCMs and modified asphalt binders

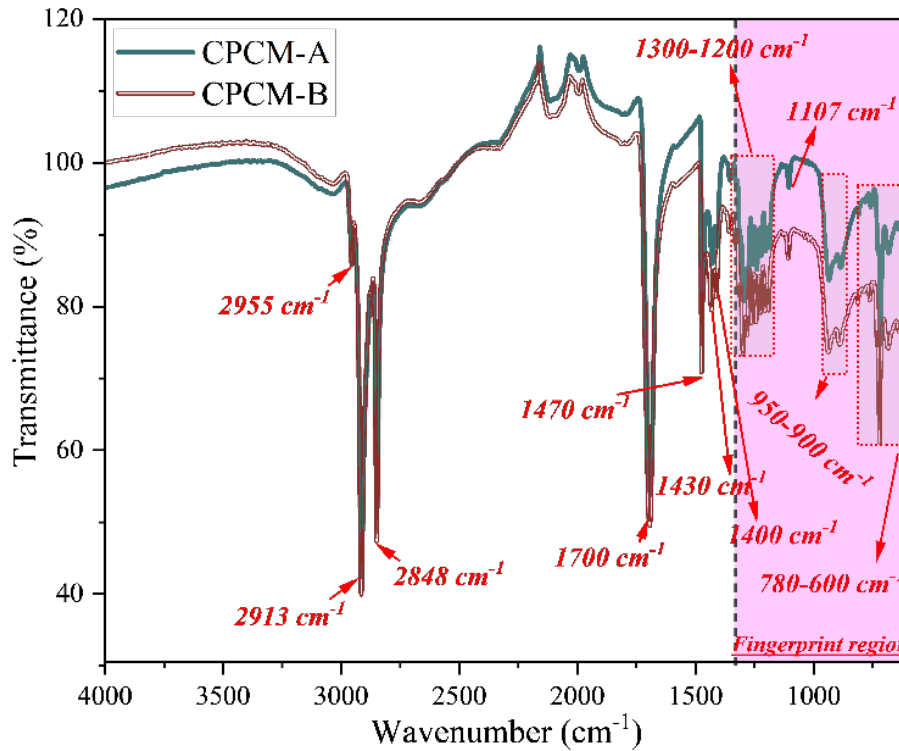
351 3.3.1 FTIR results of CPCMs

352

353 The FTIR proves to be a highly efficient instrument for investigating the chemical structure
354 of materials in terms of functional groups. The FTIR spectra of CPCMs and asphalt binders are
355 shown in Figures 8 and 9, respectively. The spectra of CPCM-A and CPCM-B exhibited
356 characteristic peaks of comparable intensity, indicating their similarity in terms of chemical
357 structure. Strong peaks were observed at 2913 cm^{-1} , 2848 cm^{-1} , and 1700 cm^{-1} , primarily attributing
358 to the alkane CH_2 anti-stretching, CH_3 symmetrical stretching, and carboxylic acid carbonyl $\text{C}=\text{O}$
359 stretching. The medium-intensity peaks at 1470 cm^{-1} and 1430 cm^{-1} corresponded to the variable
360 angle of the alkane CH_2 and the in-plane bending carboxylic acid COH , respectively. Additionally,
361 CH_3 symmetrical stretching contributed to the appearance of a weak peak at 2955 cm^{-1} . The
362 fingerprint region of the spectrum, ranging from 1330 cm^{-1} to 400 cm^{-1} , was also analyzed. The
363 vibration of the fingerprint region can be attributed to the vibration of the whole molecule or a
364 portion of the molecule and not the vibration frequency of a specific group. The peaks at $1300\text{-}1200$
365 cm^{-1} and $950\text{-}900\text{ cm}^{-1}$ aligned with the stretching and out-of-plane bending of carboxylic acid C-
366 OH . Moreover, the C-C extension of the straight chain was denoted as a weak intensity peak at 1107
367 cm^{-1} . Other absorption peaks at lower wavenumbers ($780\text{-}600\text{ cm}^{-1}$) may be ascribed to the variable-
368 angle vibrations of COO^- . Based on these results, it can be concluded that $-\text{CH}_3$, $-\text{CH}_2$, COH , and
369 $\text{C}=\text{O}$ constitute the primary constituents of CPCMs.

370 Therefore, no new characteristic peaks were inferred, signifying that no chemical reaction
371 occurred during the synthesis of CPCMs and that the adsorption of EG to eutectic PCM is incidental
372 to physical effects rather than chemical ones. Overall, these observations established that the
373 chemical properties of CPCMs correspond to those of fatty acids, demonstrating exceptional

374 chemical stability. Such stability ensures that CPCMs retain their desired properties in asphalt
375 pavement environments where consistent performance is crucial.



376

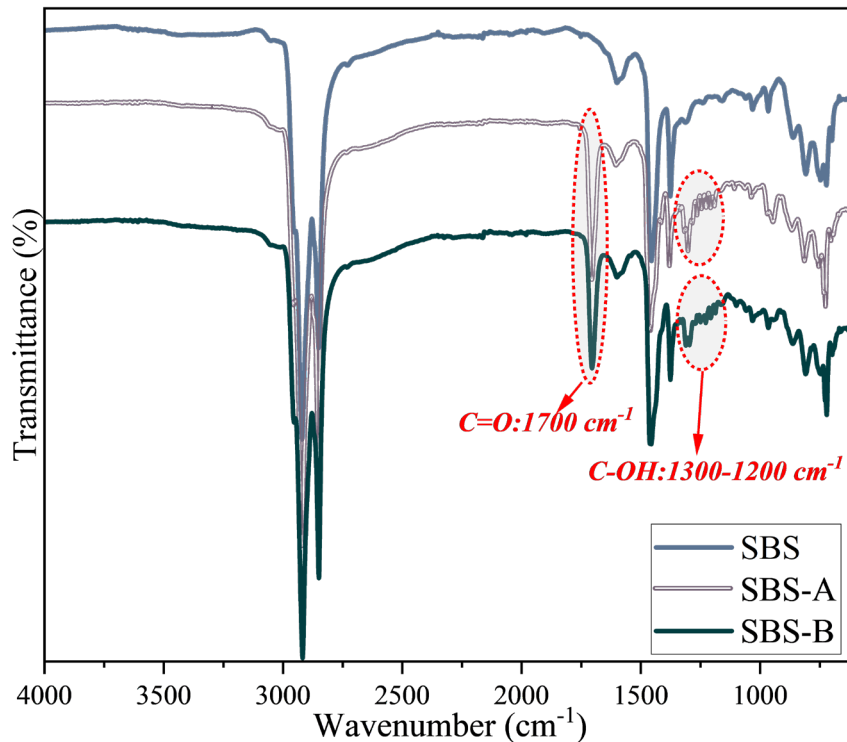
377

Figure 8 The FTIR spectrums of CPCMs

378 3.3.2 FTIR results of modified asphalt binders

379 The SBS, SBS-A, and SBS-B spectra are reported in Figure 9, underscoring the consistent
380 molecular characteristics shared by these materials. The characteristic peaks resembling those of
381 CPCMs were predominantly observed around 2900 cm⁻¹, 2850 cm⁻¹, 1470 cm⁻¹, and 1430 cm⁻¹. The
382 peak at 1610 cm⁻¹ in the three asphalt binders is attributed to the C=C stretching of the aromatic
383 ring. In addition to the absorption peaks related to SBS-modified bitumen, fatty acid properties
384 conveying absorption peaks were also evident, such as the characteristic peak at 1700 cm⁻¹ and the
385 characteristic peaks group within the range 1300-1200 cm⁻¹ (falling within the fingerprint region),
386 which were only discernible in the SBS-A and SBS-B spectra. These peaks are attributed to the
387 carboxylic acid carbonyl C=O stretching and out-of-plane bending movements of the carboxylic

388 acid C-OH. This spectral evidence indicated that CPCMs were seamlessly incorporated into the
389 asphalt binder. Significantly, when comparing with SBS, no additional absorption peaks were
390 observed apart from the characteristic peaks inherited from the CPCMs, indicating the chemical
391 stability of composite phase change asphalt binders. Noticeable chemical stability is fundamental
392 for realizing excellent thermal management performance for cooling asphalt pavement that employs
393 PCM applications. This ensures that the material's intrinsic properties remain unchanged, fostering
394 robust thermal management (Liu et al., 2020; Liu et al., 2021). These findings were further
395 confirmed by Salman et al. (Hasanabadi et al., 2021) and Dong et al. (Zhang, D. et al., 2018),
396 reinforcing the notion that incorporating CPCMs into binders without compromising their chemical
397 stability offers a potential solution for improving the performance of asphalt pavements.



398

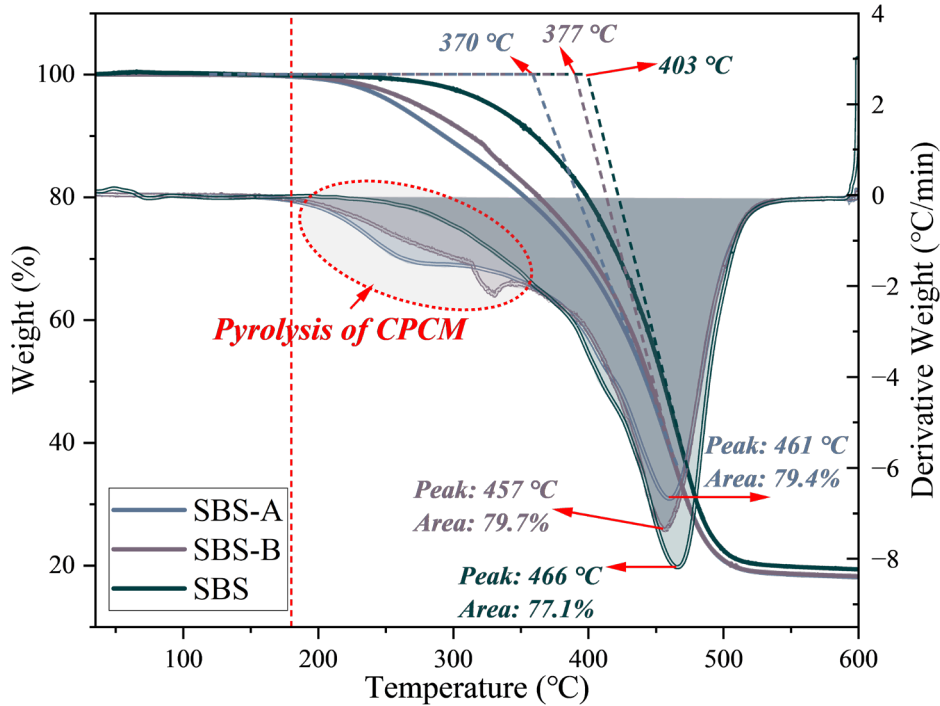
399

Figure 9 The FTIR spectrums of asphalt binders

400 3.4 Thermal stability of modified asphalt binders

401 An asphalt binder that demonstrates degradation or thermal decomposition at the production
402 temperature of hot mix asphalt mixes (i.e. 180°C approx.) could significantly compromise the
403 pavement's quality, longevity, and performance. As shown in Figure 10, SBS-A and SBS-B showed
404 no thermal decomposition before 180°C, as their masses remained equal to 100%. This is a
405 promising indicator for practical applications. Furthermore, the thermal decomposition of the
406 asphalt binders proceeded through three distinct stages: a stable decomposition stage, a rapid
407 decomposition stage, and an ultimate decomposition stage. The decomposition reaction of the
408 original SBS-modified asphalt binder started at a temperature of 230°C and reached its maximum
409 thermal decomposition rate at 466°C. The SBS-A and SBS-B displayed similar thermal
410 decomposition trends, starting their thermal decomposition reactions at 190°C and their maximum
411 thermal decomposition rates at 457°C and 461°C, respectively. Each of the three asphalt binders
412 was decomposed at approximately 500°C, leaving a remaining mass of 77.1%, 79.4%, and 79.7%,
413 respectively. These findings suggested that incorporating CPCMs into the SBS-modified asphalt
414 binder decreased thermal stability, predominantly due to the thermal decomposition of CPCMs. This
415 was evident through a faint peak between 200°C and 400°C in the derivative weight curves of SBS-
416 A and SBS-B.

417 While CPCMs were responsible for reducing the thermal stability of asphalt binders, they
418 maintained consistent mass up to 180°C, enabling SBS-modified asphalt binder with CPCMs to
419 meet the thermal stability requirements for hot mix asphalt mixtures. Consequently, the benefits
420 offered by CPCMs, such as enhanced temperature regulation, were achieved without detracting from
421 the material's foundational requirements (Jin et al., 2019; Kheradmand et al., 2015).



422

Figure 10 The TG and DTG curves of asphalt binders

423

3.5 Rheological performances of modified asphalt binders

424

3.5.1 Temperature sweep tests of modified asphalt binders

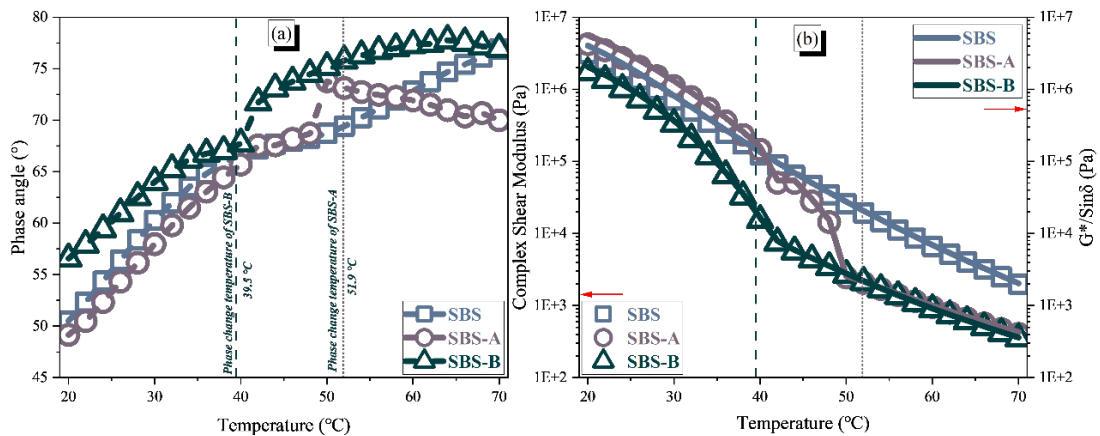
425

426 Figure 11 displays the results of the temperature sweep tests performed on the asphalt
 427 binders in the range of 20–70°C to identify the binder's thermal susceptibility. These parameters
 428 indicate the material's viscoelastic behavior and ability to withstand deformation (Jia et al., 2022).
 429 The phase angle of binders generally experiences a gradual increase while increasing temperature
 430 (Tarsi et al., 2020). The phase angle is a significant parameter that indicates the elastic proportion
 431 of a material. Specifically, it represents the tangent value of the storage and loss moduli. In an ideal
 432 scenario, the phase angle of an elastic body would be 0°, while that of a viscous body would be 90°
 433 (Zhang, H. et al., 2018). It is widely accepted that the asphalt binder undergoes a process of gradual
 434 softening with an increase in temperature, leading to a corresponding reduction in the relative elastic
 435 component. The phase angle of SBS-B was roughly 6° higher than that of both SBS and SBS-A

436 before 40 °C, and it remained higher throughout the whole temperature range of the test. This
437 difference suggested that SBS-B was less elastic than the other two binders. Until 52°C, SBS-A had
438 a phase angle comparable to SBS. As Figure 11 (a) indicates, the two distinct composite binders,
439 SBS-B and SBS-A, had melting phase-change temperatures at 40 °C and 52 °C, respectively, where
440 an apparent change in the trend of δ -T curves could be observed. This indicates that the CPCM's
441 phase-change temperature influenced the final binder's viscoelastic properties. To be specific, at the
442 corresponding phase-change temperature, a distinct increase in the phase angle was observed: from
443 68.7° to 73.8° for SBS-B and from 67.7° to 71.7° for SBS-A. Interestingly, while the phase angle
444 of SBS-B continues to increase with rising test temperature, SBS-A exhibited a reduction. Compared
445 with the previous research, it is evident that the changes in the phase angle of SBS-A align with
446 those of unencapsulated PCM asphalt composites, thereby confirming a small amount of leakage of
447 CPCM. This may be due to the precipitation of PCM caused by the shear force during the
448 preparation of the asphalt binders (Zhang, H. et al., 2018).

449 Moreover, as illustrated in Figure 11 (b), asphalt binders' complex shear modulus and rutting
450 factors ($G^*/\sin \delta$) gradually decreased, primarily due to the transition of binders from a highly elastic
451 state to a more viscous flow state with increased temperature. Also noteworthy, the phase-change
452 temperature of a CPCM was responsible for the sudden alteration of the complex shear modulus
453 and rutting factor of the two composite binders. Before phase-change, SBS-A exhibited the highest
454 complex modulus and rutting factor compared to the other two binders, indicating superior
455 resistance to deformation. Conversely, SBS-B displayed the lowest deformation resistance. For
456 instance, the complex modulus and rutting factor of SBS-A and SBS-B were approximately 3%
457 higher and 5% lower than SBS at 28°C, respectively. This phenomenon is likely due to the premature

458 phase-change of CPCMs in asphalt binders, which occurred earlier than 20°C owing to the mismatch
 459 in thermal conductivity between asphalt binder and CPCMs. Thereafter, SBS-A and SBS-B
 460 demonstrated comparable anti-deformation parameters roughly 20% lower than SBS after phase-
 461 change. The decline in resistance to deformation may be attributed to the minor leakage of CPCMs.
 462 Overall, composite asphalt binders can experience enhanced deformation and temperature
 463 susceptibility resistance with higher phase-change temperature CPCMs such as SBS-A. It should be
 464 noted, however, that the leakage of CPCMs may result in reduced deformation resistance of the
 465 binder once its phase transformation has concluded. These findings are consistent with those of
 466 Zhang et al., (Zhang et al., 2019) and Jia et al., (Jia et al., 2022), demonstrating that incorporating
 467 CPCMs improves asphalt binders' temperature-dependent characteristics.



468
 469 Figure 11 The temperature sweeps of asphalt binders: (a) phase angle, (b) complex shear modulus,
 470 and rutting factors

471 3.5.2 MSCR tests of modified asphalt binders

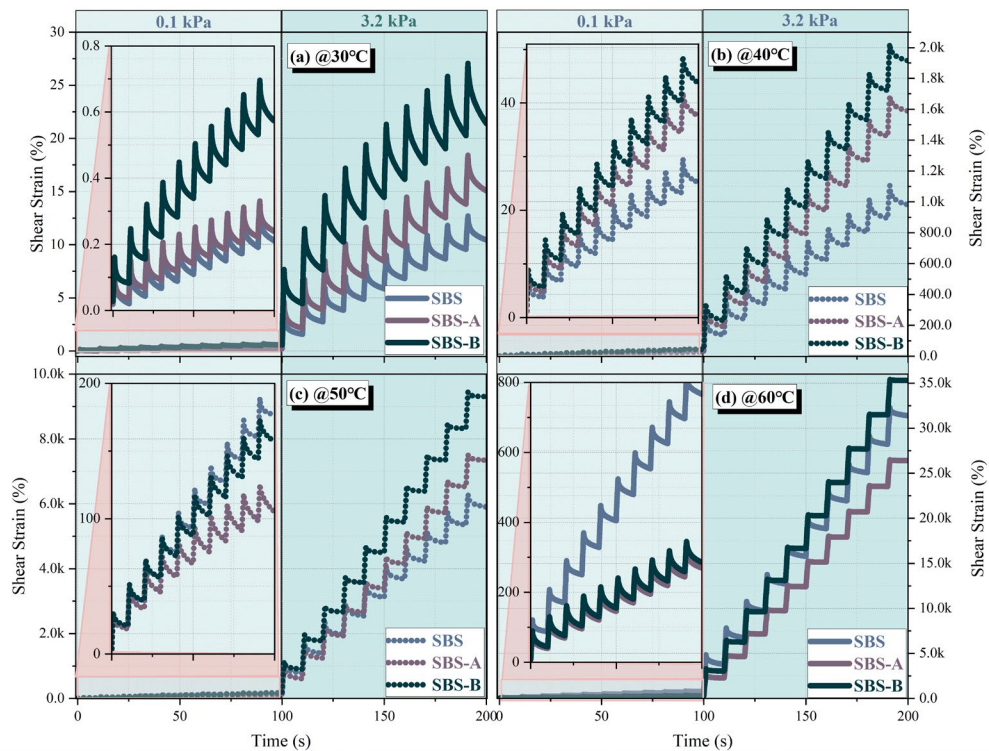
472 Figure 12 depicts the strain versus time curves of the performed MSCR tests, whereas Figure
 473 13 is a radar chart showing the four crucial parameters (i.e., $R_{3.2}$, $R_{0.1}$, $J_{nr3.2}$, and $J_{nr0.1}$) at different
 474 test temperatures. The MSCR results demonstrated that the strain differential of binders as a function
 475 of time is affected by strain level and test temperature (Jia et al., 2021). Regardless of stress level,
 476 SBS-A and SBS-B exhibited higher accumulated strains than SBS at 30°C and 40°C. Notably, SBS-

477 B experienced the most significant strain accumulation among the three binders at both stress levels.
478 For instance, the final accumulated strains of SBS-B, SBS-A, and SBS at 30°C and 0.1 kPa were
479 0.57%, 0.24%, and 0.22%, respectively. Thus, the SBS-B and SBS-A were 159.1% and 9.1% higher
480 than the control SBS. At 3.2kPa, their final accumulated strains of SBS-A and SBS-B were were
481 respectively 104% and 44.3% higher than those of SBS. These findings suggested that SBS-B may
482 negatively impact the permanent deformation resistance of asphalt binder due to its more
483 considerable cumulative strain. This reflects the more viscous-like behavior compared to SBS-A
484 and SBS highlighted from the temperature sweep tests. As anticipated, this could be attributed to
485 the faster phase change of CPCM-B. However, the strain curves showed a different trend at higher
486 temperatures, namely 50°C and 60°C. The SBS exhibited a consistently higher cumulative strain
487 than SBS-A and SBS-B, and the cumulative strain experienced at 0.1 kPa reached as high as 178.79%
488 (at 50°C) and 767.78% (at 60°C). Similarly, these results supported the superior ability of SBS-A to
489 resist high-temperature deformation than SBS and SBS-B.

490 Furthermore, to appraise the capacity of asphalt binders to endure long-term deformations
491 under repeated loads at elevated temperatures, the average non-recoverable creep compliance at the
492 two stress levels, known as J_{nr} , was utilized. Meanwhile, the elastic response of asphalt binders was
493 assessed through the average percent recovery at different stress levels, represented by R (Saboo et
494 al., 2018; Sun et al., 2019). As shown in Figure 13, the radar diagrams of MSCR parameters depicted
495 the elastic response and non-recoverable creep compliance of the asphalt binders on the horizontal
496 and vertical axes, respectively. It should be noted that lower J_{nr} denotes superior rutting resistance
497 (Jia et al., 2021). Therefore, a tall vertical axis area and a decreased horizontal axis area indicate a
498 remarkable ability for the asphalt binder to recover from creep deformation and vice versa.

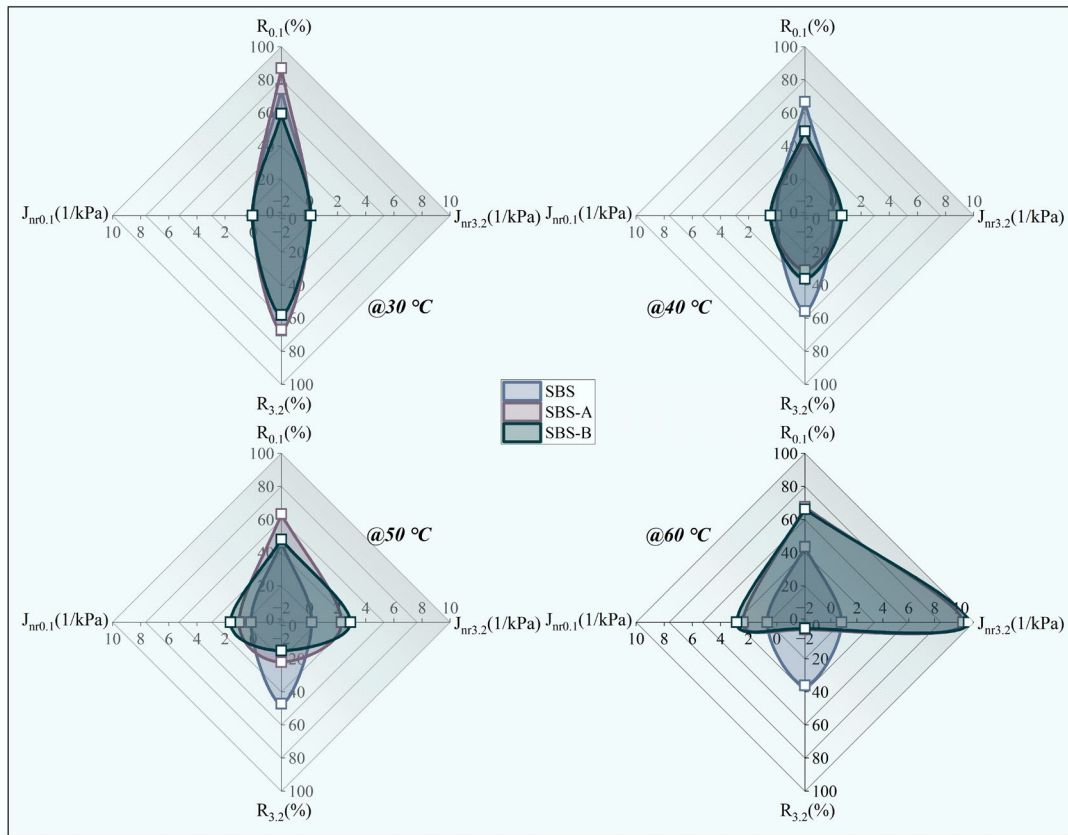
499 Generally, at 30°C and 40°C, the MSCR radar charts for each of the three binders were ideal. As
500 temperature rises, the radar map gradually evolves towards non-recoverable creep compliance.
501 Nevertheless, the radar chart of SBS consistently demonstrated that using CPCMs may harm the
502 recovery performance of asphalt binder, particularly under elevated temperatures and stress levels.
503 Specifically, SBS-A exhibited $R_{0.1}$ values approximately 18% and 37% higher than SBS at 30°C
504 and 40°C, respectively. Notably, SBS-A and SBS-B consistently displayed lower $R_{3.2}$ values and
505 higher J_{nr} values than control SBS at elevated temperatures. The $R_{3.2}$ values of SBS-A and SBS-B
506 were 15 times and 21 times lower than those of SBS, respectively, with the J_{nr} values being roughly
507 12 times higher than those of SBS (increasing from 0.8 1/kPa to 10 1/kPa).

508 To summarize, the SBS-A variant with a more significant phase transition temperature and
509 lower leakage consistently demonstrated a lower susceptibility to stress and superior recovery
510 capabilities than SBS-B.



511

512 Figure 12 The shear strain of asphalt binders at different temperatures: (a) 30 °C, (b) 40 °C, (c)
 513 50 °C, (d) 60 °C



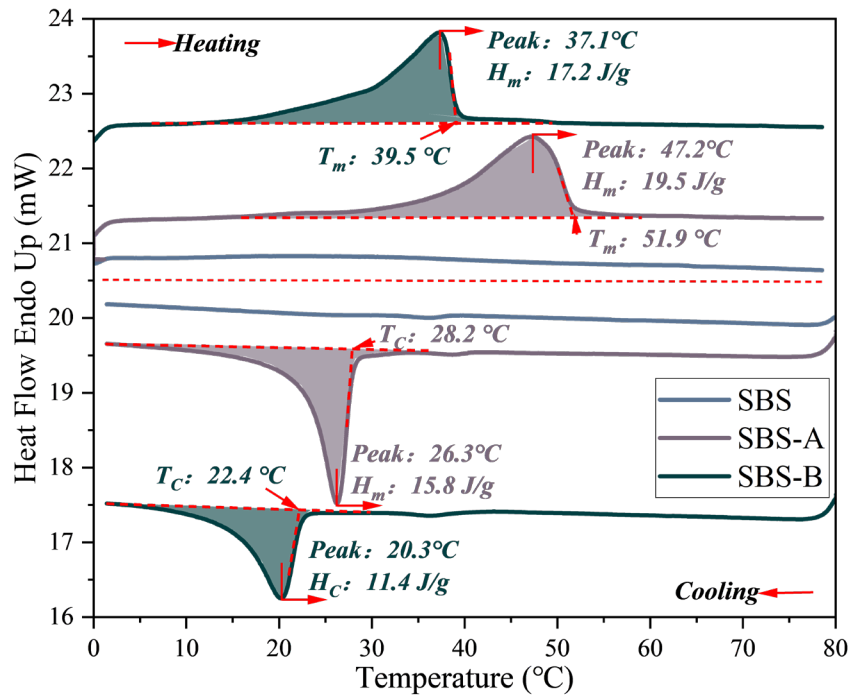
514
 515 Figure 13 The MSCR parameters of asphalt binders

516 3.6 Thermal-regulating performance of modified asphalt binders

517 3.6.1 Phase change behaviors of modified asphalt binders

518 The heat flow curves of the three asphalt binder samples obtained from the DSC analysis are
 519 illustrated in Figure 14. The SBS did not exhibit the ability to carry latent heat, precluding the
 520 detection of any endothermic or exothermic peaks during its melting and crystallization processes.
 521 Thus, it does not possess temperature regulation capabilities. Conversely, SBS-A and SBS-B
 522 displayed notable endothermic and exothermic peaks in their respective heat flow curves, which
 523 indicated the successful integration of CPCMs. It means the asphalt binders' ability to carry latent
 524 heat. The melting enthalpy for SBS-A and SBS-B was 19.5 J/g and 17.2 J/g, respectively. Comparing
 525 their theoretical values of 29.4 J/g and 28.4 J/g, respectively, the calculated phase-change efficiency

526 E (that is, the measured value of melting enthalpy/the theoretical value of melting enthalpy) of SBS-
527 A and SBS-B were approximately 66.3% and 61.6%, respectively. These phenomena could be
528 attributed to the hindrance caused by the polymer crosslinking network structure of the SBS-
529 modified asphalt binder towards the melting and crystallization of PCM. The endothermic and
530 exothermic peaks of SBS-A and SBS-B exhibited a broader range of phase-change temperatures.
531 However, the heat flow curves of asphalt binders differed from those of the corresponding CPCMs;
532 in fact, their peaks were shifted leftward. Specifically, SBS-A demonstrated melting phase-change
533 temperature and cooling phase-change temperature of 51.9°C and 28.2°C, respectively, which were
534 lower than those of CPCMs-A by 9.8°C and 33.5°C. Similarly, the melting and cooling phase change
535 temperatures of SBS-B were lower than those of CPCM-B, respectively, by 11°C and 28.7°C.
536 Additionally, SBS-A and SBS-B exhibited supercooling effects of 23.7°C and 17.1°C, respectively.
537 The decrease in phase-change temperature may be attributed to non-uniform thermal conductivity
538 between the asphalt binders and CPCMs. Higher thermal conductivity in asphalt binders resulted in
539 broader heat transfer, leading to an earlier phase-change reaction of CPCMs. Therefore, it is
540 essential to consider the impact of asphalt binder on reducing phase-change temperature and
541 enthalpy during PCM applications. The SBS-A had a higher cooling phase-change temperature than
542 SBS-B, at 28.2° C and 22.4°C, respectively. The higher cooling phase-change temperature of SBS-
543 A led the asphalt binder to be more suitable for the working environment of asphalt pavements,
544 ensuring its phase-change cycle reaction in the corresponding working environment. Consequently,
545 CPCMs endow SBS-modified asphalt binder with latent heat function to provide excellent
546 temperature regulation performance. The CPCM-A may be the appropriate choice for cooling
547 asphalt pavements compared to CPCM-B.



548

549

Figure 14 The heat flow curves of asphalt binders

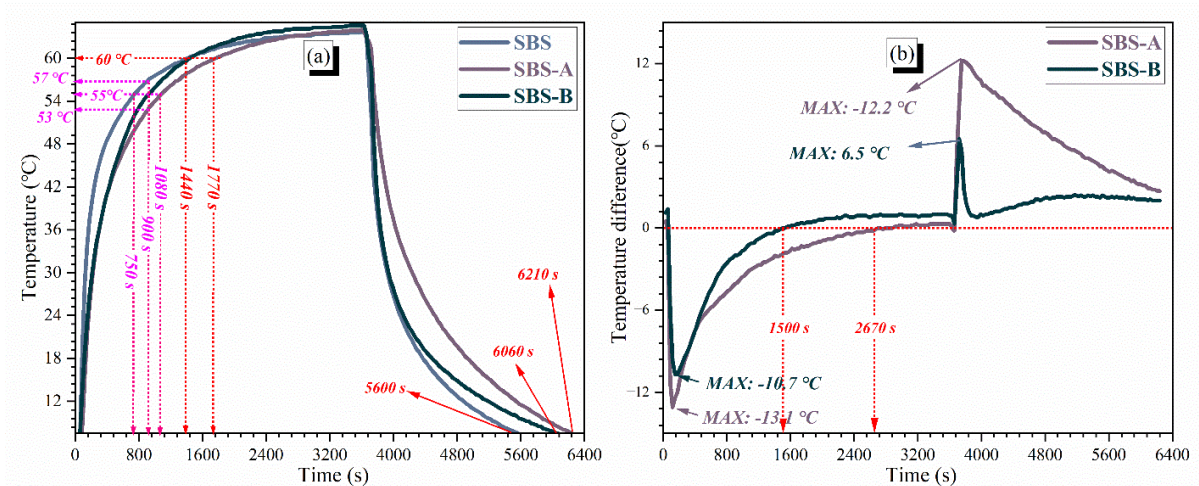
550 3.6.2 Time-temperature curves of modified asphalt binders

551 Figure 15 presents the temperature-time curves of asphalt binders during heating and cooling
 552 periods. The regulating temperature ability of various CPCMs was analyzed by assessing the
 553 duration required for different modified asphalt materials to attain the same or different temperatures
 554 when subjected to identical heating and cooling times. It can be seen from Figure 15 (a) that the
 555 three asphalt binders exhibited discernible variations in their curve shapes. The temperature curve
 556 of SBS indicated a notable variance from SBS-A and SBS-B, with consistently higher temperature
 557 readings. The SBS-A and SBS-B reached 60°C at approximately 1440 seconds, while SBS was
 558 around 1770 seconds. The disparity between the control SBS and the other two composite binders
 559 indicated a temperature lag of 330 s. This finding highlights the increased susceptibility of SBS
 560 asphalt binder to thermal shock and temperature-related deterioration after adding CPCMs.

561 Moreover, it is worth noticing that a similar trend could be observed in the temperature curves
562 of SBS-A and SBS-B, which displayed swift elevation from 8°C to 47°C within a timeframe of 600
563 s. As the heating continued, it was observed that the heating rate of SBS-B exhibited a gradual
564 increase compared to SBS-A. For instance, the temperatures recorded for SBS, SBS-A, and SBS-B
565 were 57°C, 55°C, and 53°C at 900 s. Additionally, the time required for each sample to reach 55°C
566 was 750 s, 900 s, and 1080 s, respectively. These phenomena can be attributed to the fact that
567 CPCMs endow the asphalt binder with latent heat properties. As a result, the binder accumulated
568 heat in a latent form, considerably reducing its heating rate. The phase change temperature ranges
569 of SBS-A and SBS-B were 10-40°C and 15-52°C, respectively. Once the phase change end
570 temperature was surpassed, the heat was stored in the binder as sensible heat, accounting for the
571 sudden rise in SBS-B beyond 40°C. Additionally, SBS-A consistently upheld the lowest heating rate,
572 demonstrating excellent temperature adjustment ability, mainly due to the higher phase change
573 enthalpy of CPCM-A (19.5 J/g) than that of CPCM-B (17.2 J/g). Various phase change temperatures
574 and enthalpy of CPCMs affected the cooling process. During the cooling phase, these samples
575 experienced a gradual decrease in temperature from 65°C to 8°C over 5600 s, 6060 s, and 6210 s,
576 respectively. Notably, SBS demonstrated a slower cooling rate than SBS-A and SBS-B, taking an
577 additional 610 s and 460 s, respectively, to reach an equilibrium temperature. The exothermic
578 reaction in CPCMs can be considered responsible for these findings.

579 Specifically, as shown in Figure 15 (b), during the heating process of SBS-A and SBS-B, the
580 maximum temperature difference of 13.1°C and 10.7°C was observed around 120 s and 150 s,
581 respectively. Meanwhile, SBS-A and SBS-B exhibited temperature lags of 1500 s and 2610 s,
582 respectively. Since the exothermic enthalpies of SBS-A and SBS-B were 3.7 J/g and 5.8 J/g lower

583 than the endothermic enthalpies, respectively, the maximum temperature differences observed
 584 during the cooling process were 12.2°C and 6.5°C, respectively. Overall, incorporating CPCMs into
 585 asphalt binder provided their exceptional cooling capabilities through latent heat capacity.
 586 Nevertheless, SBS-A, which boasts higher phase change temperature and enthalpy, demonstrated a
 587 better ability to regulate temperature.



588
589 Figure 15 The temperature-time curves of asphalt binders

590 4. Conclusions

591 The primary goal of this study was to create two high-enthalpy CPCMs and integrate them into
 592 SBS-modified asphalt binders to explore their latent heat potential for cool asphalt pavements.
 593 Based on the findings, the following conclusions can be drawn:

594 (1) CPCM-A and CPCM-B demonstrated high adsorption efficiencies (over 90%) and
 595 substantial melting enthalpies. Their melting temperatures and thermal stability fit the asphalt
 596 pavement construction and service requirements.

597 (2) While CPCMs improved the rheological properties of the resulting binders, there was a
 598 need for a higher phase-change temperature. Compared to SBS-A, SBS-B underwent phase-change
 599 at an earlier stage, resulting in lower resistance to deformation. Meanwhile, CPCMs increased the

600 thermal and stress susceptibility of the asphalt binders, resulting in more significant strain
601 accumulation, which may be detrimental.

602 (3) Incorporating CPCMs into SBS-modified asphalt increased its latent heat function, with
603 notable heat storage and thermal-regulating capacity. Temperature differences of 13.1°C and 10.7°C
604 were observed for SBS-A and SBS-B around 120 s and 150 s, respectively, with temperature lags
605 of 1500 s and 2610 s, emphasizing their thermal behaviors.

606 (4) The infrared spectra analyses confirmed the chemical stability of both CPCMs and asphalt
607 binders, indicating no chemical reactions during various processes. Although CPCMs marginally
608 reduced the thermal stability of asphalt binders, the final product still met the thermal stability
609 criteria for hot mix asphalt mixtures. CPCM-A emerged as a preferable choice for developing cool
610 asphalt pavements among the studied materials.

611 While this work established the promising properties of CPCM-A and CPCM-B, further
612 investigations on the encapsulation process of PCMs into the supporting materials and their long-
613 term performances are necessary. Specifically, their durability and consistency should be assessed
614 under continuous high temperatures, traffic loads, and various meteorological conditions in real-
615 road environments. Conducting a thorough assessment of the uniform dispersion, thermal storage
616 stability, and low-temperature flexibility displayed by PCMs when integrated into asphalt binders
617 holds significant importance. Beyond performance evaluations, the potential of asphalt pavements
618 using CPCMs in mitigating the UHI effect and other environmental benefits is pivotal.

619 **5. Declaration of competing interest**

620 The authors declared that they have no conflict of interest in this work.

621 **6. Acknowledgments**

622 Authors appreciate the funding support from the National Key R&D Program of China [grant
623 number 2023YFBYFB2604600], the National Natural Science Foundation of China [grant number
624 52038001], the Fundamental Research Funds for the Central Universities, Chang'an University
625 [grant number 300102213501 and CHD300102212704], and the China Scholarship Council [grant
626 number 202106560029].

627 The authors would also like to express their gratitude to the Road Pavement Section of the
628 University of Bologna for performing the experimental activities and for their valuable assistance
629 in conducting all the tests.

630 **References**

- 631 Anderson, G.B., Bell, M.L., 2011. Heat waves in the United States: mortality risk during heat waves and
632 effect modification by heat wave characteristics in 43 U.S. communities. *Environ Health Perspect* 119(2),
633 210-218.
- 634 Anupam, B.R., Sahoo, U.C., Rath, P., 2023. Effect of two organic phase change materials on the thermal
635 performance of asphalt pavements. *International Journal of Pavement Engineering* 24(1).
- 636 ASTM, 2015. Standard Test Method for Multiple Stress Creep and Recovery (MSCR) of Asphalt Binder
637 Using a Dynamic Shear Rheometer. ASTM, ASTM International, 100 Barr Harbor Drive, PO Box C700,
638 West Conshohocken, PA 19428-2959. United States.
- 639 Bai, G., Fan, Q., Song, X.-M., 2018. Preparation and characterization of pavement materials with phase-
640 change temperature modulation. *Journal of Thermal Analysis and Calorimetry* 136(6), 2327-2331.
- 641 Chen, J., Li, J., Wang, H., Huang, W., Sun, W., Xu, T., 2019. Preparation and effectiveness of composite
642 phase change material for performance improvement of Open Graded Friction Course. *Journal of Cleaner*
643 *Production* 214, 259-269.
- 644 Chen, Y., Wang, H., You, Z., Hossiney, N., 2020. Application of phase change material in asphalt mixture
645 – A review. *Construction and Building Materials* 263.
- 646 Cheng, C., Cheng, G., Gong, F., Fu, Y., Qiao, J., 2021. Performance evaluation of asphalt mixture using
647 polyethylene glycol polyacrylamide graft copolymer as solid–solid phase change materials. *Construction*
648 *and Building Materials* 300.
- 649 Dai, J., Ma, F., Fu, Z., Li, C., Jia, M., Shi, K., Wen, Y., Wang, W., 2021. Applicability assessment of
650 stearic acid/palmitic acid binary eutectic phase change material in cooling pavement. *Renewable Energy*
651 175, 748-759.
- 652 Dai, J., Ma, F., Fu, Z., Li, C., Wu, D., Shi, K., Dong, W., Wen, Y., Jia, M., 2022. Assessing the direct
653 interaction of asphalt binder with stearic acid/palmitic acid binary eutectic phase change material.
654 *Construction and Building Materials* 320.

655 Dai, J., Ma, F., Fu, Z., Liu, J., Li, C., Hou, Y., Wu, H., 2023. Effectiveness of the different eutectic phase-
656 change materials in cooling asphalt pavement. *Construction and Building Materials* 407.

657 Du, W., Fei, H., He, Q., Wang, L., Pan, Y., Liu, J., 2021. Preparation and properties of capric acid-stearic
658 acid-based ternary phase change materials. *RSC Adv* 11(40), 24938-24948.

659 Du, Y., Liu, P., Quan, X., Ma, C., Tian, J., Wu, X., 2021. Improving Rutting and Fatigue Properties of
660 Asphalt Mastic by Adding Cement–Polyethylene Glycol Composite. *Journal of Materials in Civil
661 Engineering* 33(10).

662 Du, Y., Liu, P., Wang, J., Wang, H., Hu, S., Tian, J., Li, Y., 2019. Laboratory investigation of phase change
663 effect of polyethylene glycol on asphalt binder and mixture performance. *Construction and Building
664 Materials* 212, 1-9.

665 Farnam, Y., Krafcik, M., Liston, L., Washington, T., Erk, K., Tao, B., Weiss, J., 2016. Evaluating the use
666 of phase change materials in concrete pavement to melt ice and snow. *Journal of Materials in Civil
667 Engineering* 28(4), 04015161.

668 Gong, X., Liu, Q.T., Lv, Y., Chen, S.C., Wu, S.P., Ying, H., 2023. A systematic review on the strategies
669 of reducing asphalt pavement temperature. *Case Studies in Construction Materials* 18.

670 Guo, M., Liang, M., Jiao, Y., Zhao, W., Duan, Y., Liu, H., 2020. A review of phase change materials in
671 asphalt binder and asphalt mixture. *Construction and Building Materials* 258.

672 Hailot, D., Bauer, T., Kröner, U., Tamme, R., 2011. Thermal analysis of phase change materials in the
673 temperature range 120–150°C. *Thermochimica Acta* 513(1-2), 49-59.

674 Hasanabadi, S., Sadrameli, S.M., Sami, S., 2021. Preparation, characterization and thermal properties of
675 surface-modified expanded perlite/paraffin as a form-stable phase change composite in concrete. *Journal
676 of Thermal Analysis and Calorimetry* 144(1), 61-69.

677 Hou, Y., Ma, F., Fu, Z., Li, C., An, Q., Zhu, C., Dai, J., 2023. Encapsulation of stearic-palmitic acid in
678 alkali-activated coconut shell and corn cob biochar to optimize energy storage. *Journal of Energy Storage*
679 66.

680 Hu, H., Chen, W., Cai, X., Xu, T., Cui, H., Zhou, X., Chen, J., Huang, G., Sun, Y., 2021. Study on
681 preparation and thermal performance improvements of composite phase change material for asphalt steel
682 bridge deck. *Construction and Building Materials* 310.

683 Jia, M., Sha, A., Jiang, W., Wang, W., Li, J., Dai, J., Lu, Z., 2021. Laboratory evaluation of poly(ethylene
684 glycol) for cooling of asphalt pavements. *Construction and Building Materials* 273.

685 Jia, M., Sha, A., Jiang, W., Wang, W., Yuan, D., 2023. Adhesion, rheology and temperature-adjusting
686 performance of polyurethane-based solid–solid phase change asphalt mastics subjected to laboratory
687 aging. *Materials and Structures* 56(3).

688 Jia, M., Sha, A., Jiang, W., Wang, W., Yuan, D., Li, J., Dai, J., Jiao, W., 2022. A solid–solid phase change
689 filler with enhanced thermal properties for cooling asphalt mastic. *Solar Energy* 242, 105-118.

690 Jiao, W., Sha, A., Zhang, J., Jia, M., Jiang, W., Hu, L., 2023. Design and properties of polyurethane solid–
691 solid phase-change granular temperature regulation asphalt mixtures. *Solar Energy* 253, 47-57.

692 Jin, J., Liu, L., Liu, R., Wei, H., Qian, G., Zheng, J., Xie, W., Lin, F., Xie, J., 2019. Preparation and
693 thermal performance of binary fatty acid with diatomite as form-stable composite phase change material
694 for cooling asphalt pavements. *Construction and Building Materials* 226, 616-624.

695 Jin, J., Liu, S., Gao, Y., Liu, R., Huang, W., Wang, L., Xiao, T., Lin, F., Xu, L., Zheng, J., 2021.
696 Fabrication of cooling asphalt pavement by novel material and its thermodynamics model. *Construction
697 and Building Materials* 272.

698 Jin, J., Xiao, T., Zheng, J., Liu, R., Qian, G., Xie, J., Wei, H., Zhang, J., Liu, H., 2018. Preparation and
699 thermal properties of encapsulated ceramsite-supported phase change materials used in asphalt
700 pavements. *Construction and Building Materials* 190, 235-245.

701 Kakar, M.R., Refaa, Z., Bueno, M., Worlitschek, J., Stamatiou, A., Partl, M.N., 2019a. Investigating
702 bitumen's direct interaction with Tetradecane as potential phase change material for low temperature
703 applications. *Road Materials and Pavement Design* 21(8), 2356-2363.

704 Kakar, M.R., Refaa, Z., Worlitschek, J., Stamatiou, A., Partl, M.N., Bueno, M., 2019b. Effects of aging
705 on asphalt binders modified with microencapsulated phase change material. *Composites Part B:
706 Engineering* 173.

707 Ke, H., 2017. Phase diagrams, eutectic mass ratios and thermal energy storage properties of multiple
708 fatty acid eutectics as novel solid-liquid phase change materials for storage and retrieval of thermal
709 energy. *Applied Thermal Engineering* 113, 1319-1331.

710 Kheradmand, M., Castro-Gomes, J., Azenha, M., Silva, P.D., de Aguiar, J.L.B., Zoorob, S.E., 2015.
711 Assessing the feasibility of impregnating phase change materials in lightweight aggregate for
712 development of thermal energy storage systems. *Construction and Building Materials* 89, 48-59.

713 Kolyado, A.V., Alenova, S.M., Garkushin, I.K., 2016. Phase diagram of a system of adipic, glutaric, and
714 sebacic acids. *Russian Journal of Physical Chemistry A* 90(6), 1293-1297.

715 Li, C., Zhang, B., Xie, B., Zhao, X., Chen, J., Chen, Z., Long, Y., 2019. Stearic acid/expanded graphite
716 as a composite phase change thermal energy storage material for tankless solar water heater. *Sustainable
717 Cities and Society* 44, 458-464.

718 Li, H., Harvey, J., Jones, D., 2013. Cooling Effect of Permeable Asphalt Pavement under Dry and Wet
719 Conditions. *Transportation Research Record* 2372(1), 97-107.

720 Liu, C., Yuan, Y.P., Zhang, N., Cao, X.L., Yang, X.J., 2014. A novel PCM of lauric-myristic-stearic
721 acid/expanded graphite composite for thermal energy storage. *Materials Letters* 120, 43-46.

722 Liu, Q., Wu, L., Wang, Y., Tang, N., Wang, X., Gao, L., Wang, Q., 2022. A novel functional coating with
723 2DMts/SA phase change material as filler and its pavement temperature regulation performance.
724 *Materials Letters* 306.

725 Liu, T., Guo, N., Jin, X., Tan, Y., You, Z., Cui, S., Chu, Z., Fang, C., 2023. Thermoregulation, rheological
726 properties and modification mechanism of asphalt modified with PUSSPCMs. *Construction and Building
727 Materials* 372.

728 Liu, Z., Wang, Y., Jia, J., Sun, H., Wang, H., Qiao, H., 2020. Preparation and Characterization of
729 Temperature-Adjusting Asphalt with Diatomite-Supported PEG as an Additive. *Journal of Materials in
730 Civil Engineering* 32(3).

731 Liu, Z., Wei, K., Wang, S., Ma, B., Wang, X., Shi, W., Xu, J., 2021. Effect of high-temperature-resistant
732 epoxy resin/polyethylene glycol 2000 composite stereotyped phase change material particles on asphalt
733 properties. *Construction and Building Materials* 300.

734 Ma, B., Wang, X.-q., Zhou, X.-y., Wei, K., Huang, W., 2019. Measurement and analysis of
735 thermophysical parameters of the epoxy resin composites shape-stabilized phase change material.
736 *Construction and Building Materials* 223, 368-376.

737 Ma, G., Sun, J., Xie, S., Wang, Z., Jing, Y., Jia, Y., 2018. Solid-liquid phase equilibria of stearic acid and
738 dicarboxylic acids binary mixtures as low temperature thermal energy storage materials. *The Journal of
739 Chemical Thermodynamics* 120, 60-71.

740 Ma, Y., Yang, H., Zuo, H., Zuo, Q., He, X., Chen, W., Wei, R., 2023. EG@Bi-MOF derived porous
741 carbon/lauric acid composite phase change materials for thermal management of batteries. *Energy* 272.

742 Nazir, H., Batool, M., Ali, M., Kannan, A.M., 2018. Fatty acids based eutectic phase change system for
743 thermal energy storage applications. *Applied Thermal Engineering* 142, 466-475.

744 Nwakaire, C.M., Onn, C.C., Yap, S.P., Yuen, C.W., Onodagu, P.D., 2020. Urban Heat Island Studies with
745 emphasis on urban pavements: A review. *Sustainable Cities and Society* 63.

746 Roman, K.K., O'Brien, T., Alvey, J.B., Woo, O., 2016. Simulating the effects of cool roof and PCM
747 (phase change materials) based roof to mitigate UHI (urban heat island) in prominent US cities.
748 *ENERGY* 96, 103-117.

749 Saboo, N., Kumar, R., Kumar, P., Gupta, A., 2018. Ranking the Rheological Response of SBS- and EVA-
750 Modified Bitumen Using MSCR and LAS Tests. *Journal of Materials in Civil Engineering* 30(8).

751 Salem, T., Bichara, L., 2023. Mitigation of UHI Effect with the Incorporation of PCM in Concrete
752 Pavement-Case Study: City of Rotterdam.

753 Seki, Y., İnce, Ş., Ezan, M.A., Turgut, A., Ereğ, A., 2015. Graphite nanoplates loading into eutectic
754 mixture of Adipic acid and Sebacic acid as phase change material. *Solar Energy Materials and Solar Cells*
755 140, 457-463.

756 Sun, Y., Wang, W., Chen, J., 2019. Investigating impacts of warm-mix asphalt technologies and high
757 reclaimed asphalt pavement binder content on rutting and fatigue performance of asphalt binder through
758 MSCR and LAS tests. *Journal of Cleaner Production* 219, 879-893.

759 Tarsi, G., Caputo, P., Porto, M., Sangiorgi, C., 2020. A Study of Rubber-REOB Extender to Produce
760 Sustainable Modified Bitumens. *Applied Sciences* 10(4).

761 Tyagi, V.V., Chopra, K., Kalidasan, B., Chauhan, A., Stritih, U., Anand, S., Pandey, A.K., Sari, A.,
762 Kothari, R., 2021. Phase change material based advance solar thermal energy storage systems for
763 building heating and cooling applications: A prospective research approach. *Sustain Energy Techn* 47.

764 Wang, C., Wang, Z.-H., Kaloush, K.E., Shacat, J., 2021. Cool pavements for urban heat island mitigation:
765 A synthetic review. *Renewable and Sustainable Energy Reviews* 146.

766 Wang, H., Wang, Y., Qi, M., Wang, Q., Li, X., Zhu, X., Yu, X., Liu, Z., 2021. PEG/diatomite modified
767 Asphalt Mixture with Self-Regulating temperature property. *Case Studies in Construction Materials* 15.

768 Wei, K., Liu, Z., Wang, L., Ma, B., Fan, Y., Shi, J., Cheng, P., 2022. Preparation of polyurethane solid-
769 solid low temperature PCMs granular asphalt mixes and study of phase change temperature control
770 behavior. *Solar Energy* 231, 149-157.

771 Wu, L., Liu, Q., Tang, N., Wang, X., Gao, L., Wang, Q., Lv, G., Hu, L., 2022. Development of two-
772 dimensional nano Mts/SA phase change materials for self-adjusting temperature of pavement.
773 *Construction and Building Materials* 349.

774 Yang, L., Cao, X., Zhang, N., Xiang, B., Zhang, Z., Qian, B., 2019. Thermal reliability of typical fatty
775 acids as phase change materials based on 10,000 accelerated thermal cycles. *Sustainable Cities and*
776 *Society* 46.

777 Ye, H., Long, L., Zhang, H., Zou, R., 2014. The performance evaluation of shape-stabilized phase change
778 materials in building applications using energy saving index. *Applied Energy* 113, 1118-1126.

779 Yinfei, D., Pusheng, L., Jiacheng, W., Hancheng, D., Hao, W., Yingtao, L., 2020. Effect of lightweight
780 aggregate gradation on latent heat storage capacity of asphalt mixture for cooling asphalt pavement.
781 *Construction and Building Materials* 250.

782 Yuan, D., Jiang, W., Sha, A., Xiao, J., Wu, W., Wang, T., 2023a. Technology method and functional
783 characteristics of road thermoelectric generator system based on Seebeck effect. *Applied Energy* 331.

784 Yuan, D., Jiang, W., Xiao, J., Ling, X., Zhang, Y., Lu, R., 2023b. Experimental study on the temperature-
785 regulating function of road thermoelectric generator system. *Journal of Cleaner Production* 384.

786 Zhang, D., Chen, M., Wu, S., Liu, P., 2021. Effect of expanded graphite/polyethylene glycol composite
787 phase change material (EP-CPCM) on thermal and pavement performance of asphalt mixture.
788 *Construction and Building Materials* 277.

789 Zhang, D., Chen, M., Wu, S., Liu, Q., Wan, J., 2018. Preparation of expanded graphite/polyethylene
790 glycol composite phase change material for thermoregulation of asphalt binder. *Construction and*
791 *Building Materials* 169, 513-521.

792 Zhang, D., Chen, M.Z., Wu, S.P., Riara, M., Wan, J.M., Li, Y.Y., 2019. Thermal and rheological
793 performance of asphalt binders modified with expanded graphite/polyethylene glycol composite phase
794 change material (EP-CPCM). *Construction and Building Materials* 194, 83-91.

795 Zhang, D.R., Sani, B.M., Xu, P.X., Liu, K., Gu, F., 2023. Preparation and characterization of binary
796 eutectic phase change material laden with thermal conductivity enhancer for cooling steel slag asphalt
797 pavement. *Construction and Building Materials* 388.

798 Zhang, H., Chen, Z., Xu, G., Shi, C., 2018. Evaluation of aging behaviors of asphalt binders through
799 different rheological indices. *Fuel* 221, 78-88.

800 Zhang, J., Dong, Z., Sun, G., Qi, Y., Zhu, X., Li, Y., 2023. Roles of phase change materials on the
801 morphological, physical, rheological and temperature regulating performances of high-viscosity
802 modified asphalt. *Sci Total Environ* 875, 162632.

803